## Journal of Materials Chemistry A



#### **PAPER**



Cite this: *J. Mater. Chem. A*, 2019, **7**, 2619

# Atomistic understanding of structural evolution, ion transport and oxygen stability in layered NaFeO<sub>2</sub>†

Yurui Gao, Da Zhaoxiang Wang Dbc and Gang Lu \*\*

 $\alpha$ -NaFeO<sub>2</sub> shares a structure similar to many layered electrode materials in Li-ion and Na-ion batteries. In this work, first-principles calculations are carried out to gain atomistic understanding of structural evolution, ion transport and oxygen stability in NaFeO<sub>2</sub>. Based on the calculation results, we provide an atomistic description of phase transition and structural changes during the charging process. Meanwhile, we identify a di-vacancy assisted diffusion mechanism for Na ions and estimate the diffusion barrier that agrees with experimental data. Furthermore, we reveal that lattice strains could modulate both ion transport and oxygen stability in NaFeO<sub>2</sub>. A moderate 3% tension in the out-of-plane direction could render the ion diffusion barrierless. Moreover, it is predicted that in-plane compressions can stabilize oxygen and suppress oxygen evolution at high potentials. Thus, a combination of the out-of-plane tension with the in-plane compression is expected to reduce the diffusion barrier and stabilize oxygen simultaneously.

Received 8th November 2018 Accepted 12th January 2019

DOI: 10.1039/c8ta10767j

rsc.li/materials-a

#### 1. Introduction

Recent crises in energy and environment has prompted intense research and development of renewable energy technologies, among which energy storage is of critical importance. Sodium (Na)-ion batteries (SIBs) are drawing particular attention as potential power sources thanks to the abundance of Na in seawater and the Earth's crust. Several common electrode materials in SIBs1-6 have been studied and their structural resemblance to the electrode materials in Li-ion batteries (LIBs) has been explored. Among them, layered oxides with a formula of A<sub>x</sub>MO<sub>2</sub> are of great interest. Here A represents an alkali metal ion and M can be either one or more transition metal ions. Most of this oxide family consists of  $(MO_2)_n$  sheets formed by edgesharing MO<sub>6</sub> octahedrons, between which the alkali ions are inserted or intercalated into an octahedral (O), tetrahedral (T) or prismatic (P) motif of oxygen ions. According to the stacking order of the  $(MO_2)_n$  sheets, the layered oxides can be further categorized as O2, O3, and P3 structures, etc.7

Among the layered  $A_xMO_2$ ,  $\alpha$ -NaFeO<sub>2</sub> is of particular interest because of its low cost, nontoxicity and the fact that it has been

widely used as a prototypical model for this class of materials. <sup>8,9</sup> In  $\alpha$ -NaFeO<sub>2</sub>, (FeO<sub>2</sub>)<sub>n</sub> sheets arrange themselves in the O3 structure with ABCABC stacking. The theoretical specific capacity of NaFeO<sub>2</sub> can reach 241 mA h g<sup>-1</sup> by assuming that all the Na ions can be extracted. It has been reported that  $\alpha$ -NaFeO<sub>2</sub> can deliver a stable and reversible specific capacity of 85 mA h g<sup>-1</sup> and exhibits a flat voltage plateau at 3.3 V with a charging voltage cutoff of 3.4 V  $\nu$ s. Na<sup>+</sup>/Na. <sup>10-13</sup> However, its Coulombic efficiency at the first cycle is relatively low and the capacity retention remains unsatisfactory. Moreover, its performance significantly deteriorates when NaFeO<sub>2</sub> is charged to a higher voltage above 3.5 V, and the material becomes electrochemically inactive when charged to 4.5 V. <sup>11</sup>

Much progress has been made to elucidate redox reaction mechanism and corresponding structural evolutions in  $\alpha$ -NaFeO<sub>2</sub>. For example, it has been found that NaFeO<sub>2</sub> undergoes Fe<sup>3+</sup>/Fe<sup>4+</sup> redox reaction during the charge/discharge cycles accompanied by the formation of a monoclinic phase (Na<sub>0.5</sub>FeO<sub>2</sub>, C2/m). Furthermore, Lee<sup>16</sup> et al. reported a continuous evolution from the hexagonal O3 ( $R\bar{3}m$ ) to O''3 ( $R\bar{3}m$ ) and to monoclinic C2/m phases during the charge/discharge process. They also revealed that Fe<sup>4+</sup> species can be spontaneously reduced to Fe<sup>3+</sup>, in conjunction with the oxidation of the electrolyte, which leads to lowed Coulombic efficiency and increased electrode impedance. More recently, the structural transition from O3 ( $R\bar{3}m$ ) to monoclinic C2/m was confirmed in NaFeO<sub>2</sub> by *in situ* X-ray diffraction and its connection to the redox reactions has been examined.<sup>17</sup>

Despite the intense research on NaFeO<sub>2</sub> in the past decades, some fundamental questions remain to be answered. For

<sup>&</sup>lt;sup>a</sup>Department of Physics and Astronomy, California State University Northridge, Northridge, California 91330-8268, USA. E-mail: ganglu@csun.edu

<sup>&</sup>lt;sup>b</sup>Key Laboratory for Renewable Energy, Beijing Key Laboratory for New Energy Materials and Devices, Institute of Physics, Chinese Academy of Sciences, Beijing 100190, China

School of Physical Sciences, University of Chinese Academy of Sciences, Beijing 100190, China

<sup>†</sup> Electronic supplementary information (ESI) available. See DOI: 10.1039/c8ta10767j

example, the structural evolution at the atomic scale during the charge/discharge process is yet to be elucidated. The atomistic mechanism of ion transport in NaFeO2 has not been established. Oxygen stability at high potentials is crucial to the capacity decay of the electrode, but strategies to stabilize oxygen are still lacking. Although the presence of lattice strain is ubiquitous during the charge/discharge process, its effect on the electrochemical performance of NaFeO2 has not been explored. As well know, theoretical calculations, modeling and simulations can provide insight into fundamental process that are not otherwise accessible, and has become an integral part of material design. 18-22 In this work, we aim to bridge these gaps by first-principles investigations. More specifically, we provide an atomistic scale understanding of the structural evolution during the charge/discharge process. We elucidate the atomistic mechanism by which Na ion transport takes place. The diffusion energy barrier inferred from the proposed mechanism matches the experimental data. We examine how lattice strains could modulate ion transport and oxygen stability in NaFeO<sub>2</sub>. In particular, we discover that 3% tensile strain in the out-of-plane direction could render the ion transport barrierless, leading to ultrafast rate performance. Furthermore, we predict that the inplane compressions can stabilize oxygen and suppress oxygen evolution at high potentials.

#### 2. Computational methodology

Spin-polarized density functional theory (DFT)<sup>23,24</sup> calculations implemented in Vienna Ab-initio Simulation Package (VASP) are performed with the projector-augmented-wave pseudopotentials<sup>25,26</sup> and Perdew–Burke–Ernzerhof<sup>27</sup> exchange-correlation functional. Na (3s), Fe (3d, 4s) and O (2s, 2p) orbitals are treated as valence states. The DFT + U approach<sup>28</sup> is used to account for the strongly correlated d-electrons in (FeO<sub>2</sub>)<sub>n</sub>. The choice of *U* is described below. The cutoff energy of plane-wave basis is set at 500 eV. The nudged elastic band (NEB) method<sup>29–31</sup> is used to calculate the diffusion energy barrier of Na ion.

The charging of NaFeO<sub>2</sub> is modeled by varying x value in a Na<sub>x</sub>FeO<sub>2</sub> supercell. For Na<sub>x</sub>FeO<sub>2</sub> in  $R\bar{3}m$  structure (Fig. 1A) with

x=1 and 0.67, we use a  $3\times3\times1$  supercell (27 Na<sub>x</sub>FeO<sub>2</sub> units). To model Na<sub>x</sub>FeO<sub>2</sub> in C2/m structure (Fig. 1B) with x=0.33 and 0.5, a  $2\times3\times2$  supercell (24 Na<sub>x</sub>FeO<sub>2</sub> units) is used. For each x, we have to consider all possible arrangements of Na vacancies in Na<sub>x</sub>FeO<sub>2</sub> and identify the lowest energy configuration. This configuration represents the ground state structure corresponding to a particular charging state. A  $\Gamma$ -centered k-point mesh of  $2\times2\times1$  and  $2\times3\times2$  is used in the  $R\bar{3}m$  and C2/m supercells, respectively.

#### 3. Results and discussion

#### 3.1 Calibration of U

In this work, we choose U value according to the desodiation voltage V of NaFeO<sub>2</sub>, which is calculated as:

$$V = \frac{E(\text{Na}_x \text{FeO}_2) - E(\text{NaFeO}_2) + (1 - x)E(\text{Na})}{(1 - x)e}$$
(1)

Here  $E(\text{NaFeO}_2)$ ,  $E(\text{Na}_x\text{FeO}_2)$  and E(Na) represent the total energy of NaFeO<sub>2</sub>, dis-intercalated Na<sub>x</sub>FeO<sub>2</sub> and metallic Na, respectively. Because the experimental charging potential exhibits a rather flat plateau for 0.67 < x < 1,  $^{17}$  we consider this voltage the most appropriate to calibrate U. More specifically, we choose x = 0.67 in eqn (1) to calculate the corresponding voltage, which depends on U as shown in Fig. 1C. With U = 5.2 eV, we obtain V = 3.30 V, which matches the experimental voltage plateau value. Hence U = 5.2 eV will be used in the DFT + U calculations. Note that this U value is comparable to those reported by others for similar oxides.  $^{32,33}$ 

#### 3.2 Diffusion mechanism of Na in NaFeO<sub>2</sub>

Diffusion mechanism of Na ions is crucial to the rate performance of NaFeO<sub>2</sub>. As Na ions occupy the octahedral sites in the Na layer, the diffusion energy barriers between two adjacent octahedral sites are calculated to estimate the diffusion kinetics. In all calculations, the final site is assumed to be a Na vacancy. If there is no additional Na vacancy, the diffusion path between the two adjacent sites is found to be a straight-line, and the corresponding energy barrier is 0.79 eV (Fig. 2A). This value is much higher than the experimental value of 0.31 eV.<sup>15</sup>

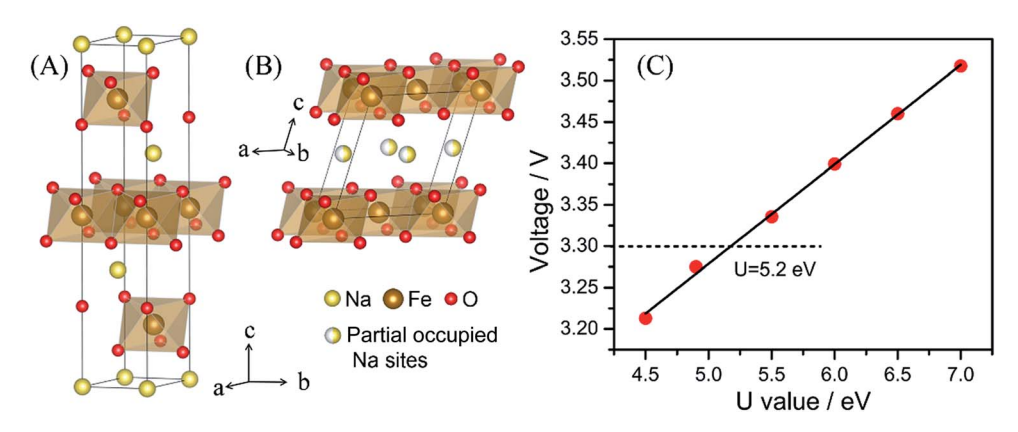


Fig. 1 The unit cells of  $Na_xFeO_2$  in R3m structure (x > 0.5, (A)) and in C2/m structure ( $x \le 0.5$ , (B)); the charging voltage (C) as a function of U in  $NaFeO_2$ .

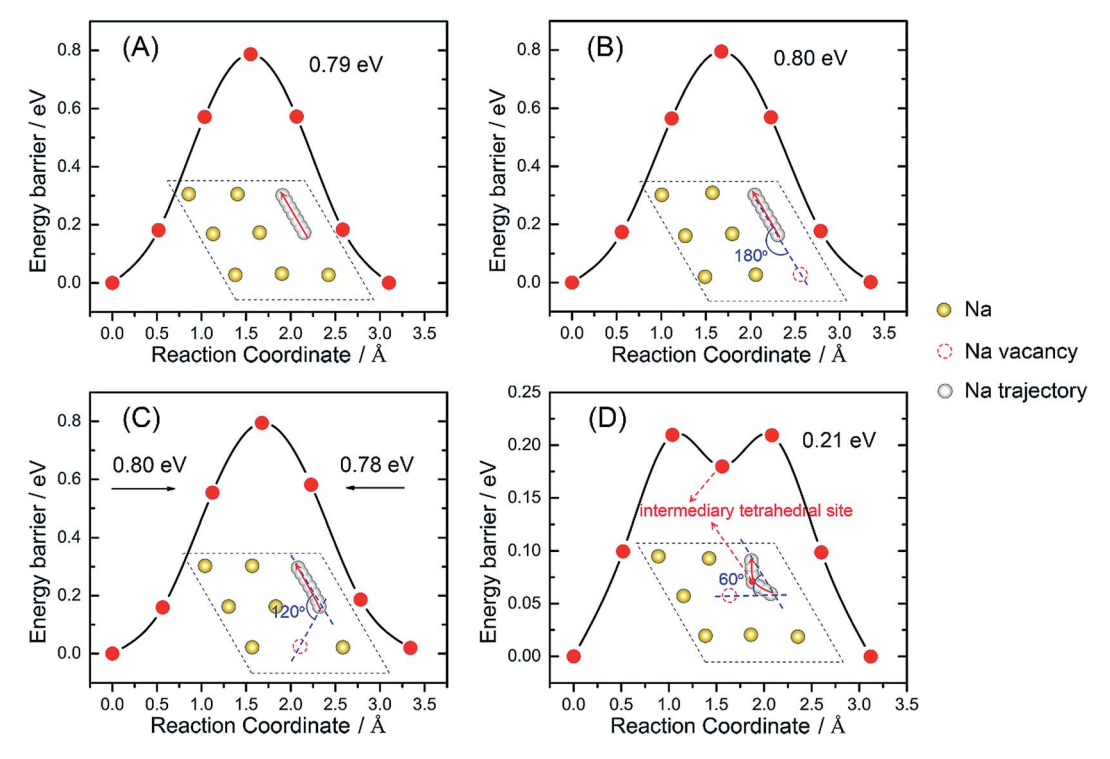


Fig. 2 Diffusion energy barrier of Na ion between two adjacent octahedral sites in NaFeO<sub>2</sub> without a nearby Na vacancy (A) and with a nearby Na vacancy (B-D). The red arrows connecting the two octahedral sites denote the diffusion pathways.

Therefore, we speculate that additional vacancies may be present in assisting the diffusion of Na ions, as examined next.

We have considered three non-equivalent configurations in which an additional vacancy is introduced at the adjacent octahedral site of the diffusing Na ion, as shown in Fig. 3B to D. For the first configuration in Fig. 2B, the energy barrier (0.80 eV) and the diffusion path are similar to those in Fig. 2A in the absence of the additional vacancy. For the second configuration

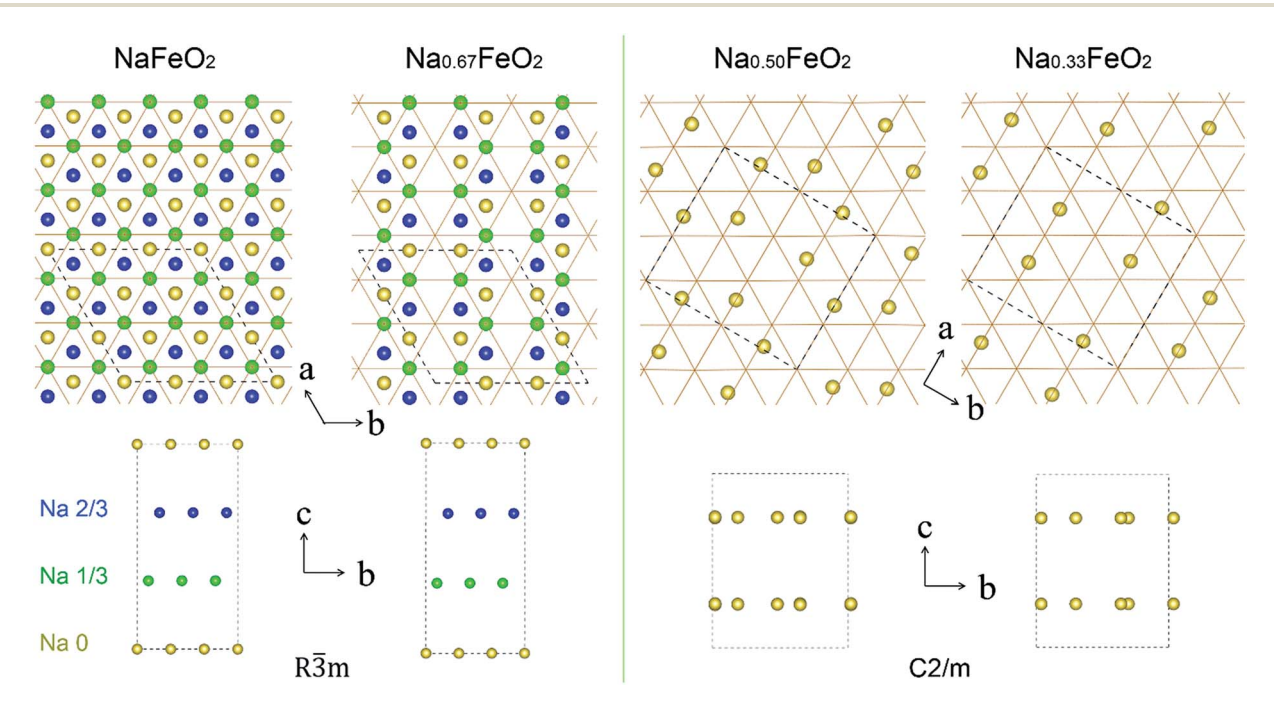


Fig. 3 Arrangements of Na ions in the lowest-energy configurations of  $Na_x FeO_2$  (x = 1, 0.67, 0.5 and 0.33) viewed along the c direction (upper panel) and along the a direction (lower panel). Different Na layers in NaFeO<sub>2</sub> and Na<sub>0.67</sub>FeO<sub>2</sub> are shown in different colors. Fe and O atoms are not shown for clarity. The vertices of each orange triangle are occupied by Fe ions.

shown in Fig. 2C, we find that the pathway is slightly curved with the similar energy barrier to that in Fig. 2A and B. For the third configuration in Fig. 2D, however, the energy barrier drops precipitously to 0.21 eV. The corresponding pathway is curved towards the vacancy via an intermediary tetrahedral site, which is made possible by the presence of the vacancy. This planar octahedral-tetrahedral-octahedral diffusion pathway is similar to the diffusion pathway of A in  $A_r(In_rSn_{1-r})O_2$  (A = Na and K) reported by Delmas.34 This pathway is also similar to the tetrahedral-site-hop mechanism in LixCoO2 proposed by Van der Ven. 35,36 Since this diffusion barrier of 0.21 eV is close to the experimental value,15 the mechanism shown in Fig. 2D is likely to be operative in NaFeO<sub>2</sub>. In other words, appropriate amount of Na vacancies is probably beneficial to the rate performance. Furthermore, we can estimate the diffusion coefficient (D) according to the following equation:

$$D = \frac{1}{n} l^2 v_0 \exp\left(-\frac{E_a}{k_b T}\right). \tag{2}$$

Here, n=4 for the 2D diffusion in layered NaFeO<sub>2</sub>; l is the hopping distance;  $E_{\rm a}$  is the diffusion barrier (0.21 eV);  $k_{\rm b}$  is the Boltzmann constant, T is the temperature, and  $\nu_{\rm 0}$  is the characteristic vibration frequency ( $\sim 10^{13}$  Hz). With these parameters, we estimate the diffusion coefficient as  $4.5 \times 10^{-6}$  cm<sup>2</sup> s<sup>-1</sup> at 300 K.

#### 3.3 Structural evolution during desodiation

It is known that during the charging process, NaFeO<sub>2</sub> undergoes a phase transition from hexagonal  $R\bar{3}m$  phase to monoclinic C2/m phase at half Na extraction. However, the corresponding atomistic structural evolution is not clear. In the following, we carry out first-principles calculations by considering three typical desodiation stages: Na<sub>0.5</sub>FeO<sub>2</sub> (half extraction), and Na<sub>0.67</sub>FeO<sub>2</sub> and Na<sub>0.33</sub>FeO<sub>2</sub> as representatives for less and more than the half extraction, respectively. Hence, Na<sub>0.67</sub>FeO<sub>2</sub> is modeled in the  $R\bar{3}m$  structure while Na<sub>0.5</sub>FeO<sub>2</sub> and Na<sub>0.33</sub>FeO<sub>2</sub> in the C2/m structure.

Our goal is to determine the lowest-energy configuration of the three representative stages. To this end, we consider all possible arrangements of Na ions in a single Na layer of Na<sub>x</sub>-FeO<sub>2</sub>. In total, 28, 462 and 330 different configurations of the inner-layer Na ions are considered for x=0.67, 0.5 and 0.33, respectively, and the lowest energy arrangement of Na ions for each x is identified. Here we assume that each Na layers takes the identical arrangement, which is justified in an ideal and uniform charging condition. Furthermore, we consider the relative shifts between the Na layers for each stage, but find negligible energy difference ( $\sim$ 4.5 meV/f.u.) between the shifts, owing to the large distances between the layers. The final atomic structures corresponding to the lowest-energy configurations of Na<sub>x</sub>FeO<sub>2</sub> (x=0.67, 0.5 and 0.33) are shown in Fig. 3. The dashed lines in Fig. 3 outline the supercells used in the calculations.

In NaFeO<sub>2</sub> ( $R\bar{3}m$ ), Na ions arrange themselves uniformly in each layer, occupying the vertices of three sets of translated equilateral triangles. The extraction of 0.33 Na (Na<sub>0.67</sub>FeO<sub>2</sub>) involves removing one Na ion in the a and b directions for every

three Na ions, forming three sets of shifted hexagons. The resultant pattern of Na ions resembles that of Mn ions in  $\text{Li}_2\text{MnO}_3$ . From  $\text{Na}_{0.67}\text{FeO}_2$  to  $\text{Na}_{0.5}\text{FeO}_2$ , the phase transition from the hexagonal  $(R\bar{3}m)$  to the monoclinic (C2/m) structure takes place, and the remaining Na ions adopt an on-top stacking in the c-direction. Further desodiation to  $\text{Na}_{0.33}\text{FeO}_2$  does not yield significantly different structural changes.

We next pay attention to the changes of the structural motifs (Fig. 4). As x is reduced from 1 to 0.33, we find that the distance between the two adjacent Fe layers (or Na layers), d, increases from 5.37 to 5.74 Å (or 7% increase, Table 1S†) while the area (per Fe ion) in the ab-plane shrinks slightly. Moreover, the thickness of the FeO<sub>6</sub> motif ( $d_1$ ) decreases while the thickness of the NaO<sub>6</sub> motif ( $d_2$ ) increases. This is due to the fact that as the positively charged Na ions are extracted, the net repulsion acting on the O layers increases, thus  $d_2$  is increased. At the same time, the valence of Fe ions rises from +3 to +4, increasing the attraction between Fe and O ions, thus  $d_1$  decreases. We find that the increase in  $d_2$  overcompensates the decrease of  $d_1$ , hence d (= $d_1$  +  $d_2$ ) increases as Na is removed. The "abnormal" volume expansion as Na is removed from NaFeO<sub>2</sub> resembles that observed in NaNbO<sub>2</sub>.<sup>37</sup>

### 3.4 Effects of lattice strain on ion transport and oxygen stability

In the following, we examine the effect of strains on Na transport in NaFeO<sub>2</sub>. We apply a uniaxial strain in the *c*-direction ( $\varepsilon = \Delta c/c$ ), ranging from -6.25% (compression) to +6.25% (tension) and a biaxial strain in the *ab*-plane ( $\varepsilon = \Delta a/a = \Delta b/b$ ) from -5% to +5%. Note that the applied strains are not large enough to induce obvious structural transitions in Na<sub>x</sub>FeO<sub>2</sub>. We have examined the energetics of the sliding of FeO<sub>2</sub> slab in Na<sub>x</sub>FeO<sub>2</sub> and found that the O3 stacking structure remains stable under the strains (Fig. 1S†). Moreover, the  $R\bar{3}m$  structure at x=1 and 0.67 or the C2/m structure at x=0.5 and 0.33 can be maintained under most strains.

Based on the vacancy-assisted diffusion mechanism shown in Fig. 2D, we calculate the diffusion energy barrier in NaFeO<sub>2</sub> as a function of the strain using the NEB method (Fig. 5 and Table 2S†). We find that the in-plane biaxial tension decreases

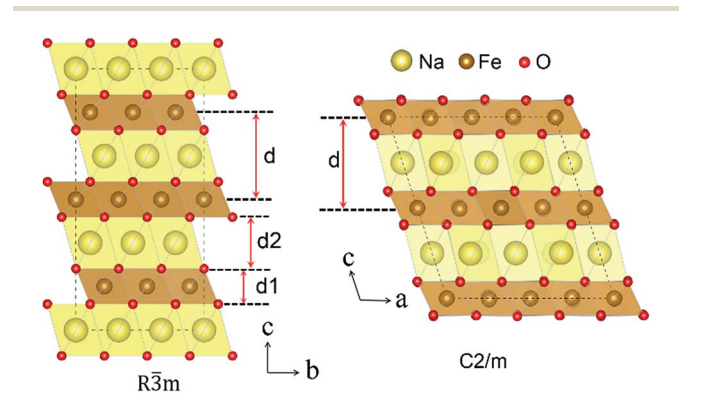


Fig. 4 The supercells used in the calculations for the R3m structure (left) and C2/m structure (right) for  $Na_xFeO_2$ .

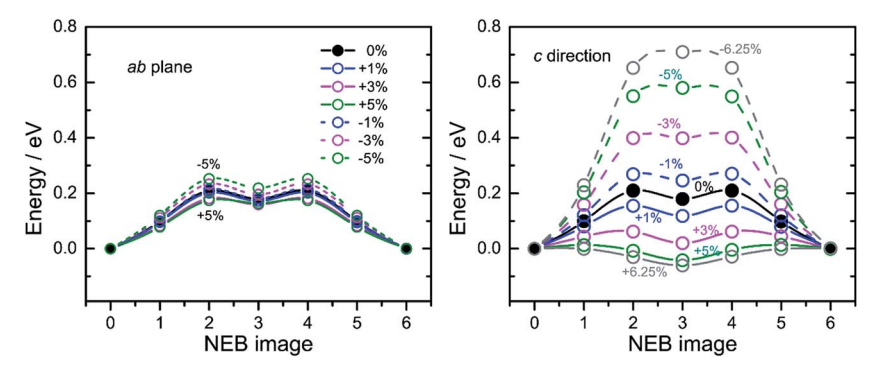


Fig. 5 The diffusion energy barrier of Na ions in NaFeO<sub>2</sub> in the presence of biaxial strains in the ab plane (left) and of the uniaxial strain in the cdirection (right). The positive or negative value of strain represents tension or compression, respectively.

the energy barrier while the compression increases it. However, the magnitude of the changes is rather small, less than 0.04 eV. In contrast, the uniaxial strain in the c-direction has a much greater effect on the diffusion energy barrier. The uniaxial tension is found to reduce the energy barrier while the compression increases it. Remarkably, 3% or greater tension in the c-direction could render the diffusion barrierless. A close look at the out-of-plane displacement of the structural motifs indicates that most of the tension is localized in the NaO2 slabs containing the Na vacancies. In other words, the tension is magnified in the slab where the vacancy-assisted diffusion takes place, yielding a much reduced energy barrier.

The stability of oxygen during de-intercalation is critical to electrochemical performance, and the instability of oxygen can lead to oxygen release, causing problems such as irreversible structure transition, voltage decay and performance deterioration.38-40 The instability of oxygen at high charging potentials in NaFeO2 has been observed in our previous work.17 Here, we extend the previous work and examine the effect of lattice strains on the oxygen stability in NaFeO2 during Na extraction. More specifically, for each applied strain, we calculate the Gibbs free energy change ( $\Delta G$ ) for the following reaction, i.e.,  $O_2$ evolution from NaFeO2, at different desodiation stages:

$$Na_x FeO_2 \rightarrow Na_x FeO_{2-\delta} + \frac{\delta}{2}O_2$$
 (3)

For eqn (3), the reaction enthalpy can be calculated according to the following equation:

$$\Delta H = \left[ E(\text{Na}_x \text{FeO}_{2-\delta}) + \frac{\delta}{2} E(\text{O}_2) - E(\text{Na}_x \text{FeO}_2) \right] / (0.5\delta) \quad (4)$$

Here,  $E(Na_xFeO_{2-\delta})$ ,  $E(Na_xFeO_2)$  and  $E(O_2)$  are the total energy of  $Na_xFeO_{2-\delta}$ ,  $Na_xFeO_2$  and  $O_2$ , respectively. The structure of oxygen-deficient  $Na_x FeO_{2-\delta}$  is obtained by removing an oxygen atom, which has the least amount of negative charge, from the ground-state configuration of Na<sub>x</sub>FeO<sub>2</sub>; the structure is then relaxed to compute  $E(Na_xFeO_{2-\delta})$ . Considering the entropy of  $O_2$ gas at the standard conditions, e.g.,  $-T\Delta S = -0.63$  eV, 1 bar and 298 K,41,42 the reaction Gibbs free energy of O2 release can be estimated. The results of  $\Delta G$  are shown in Fig. 6A and B as a function of the biaxial strain in the ab-plane and the uniaxial strain in the c-direction. In the absence of strain, as Na is removed from NaFeO<sub>2</sub>,  $\Delta G$  decreases, suggesting that oxygen becomes less stable. When  $\Delta G$  turns negative, the release of  $O_2$ is considered spontaneous. Thus, in the absence of strain, the oxygen evolution is exothermic when  $x \le 0.4$ . In the presence of in-plane biaxial strains, we find that compression tends to stabilize oxygen while tension destabilizes it. For example, in the presence of 3% compression, oxygen remains stable as long as  $x \le 0.33$ . However, under 3% tension, oxygen becomes unstable as soon as x is less than 0.5. In other words, one can tune the stability of oxygen by the in-plane strains. On the other

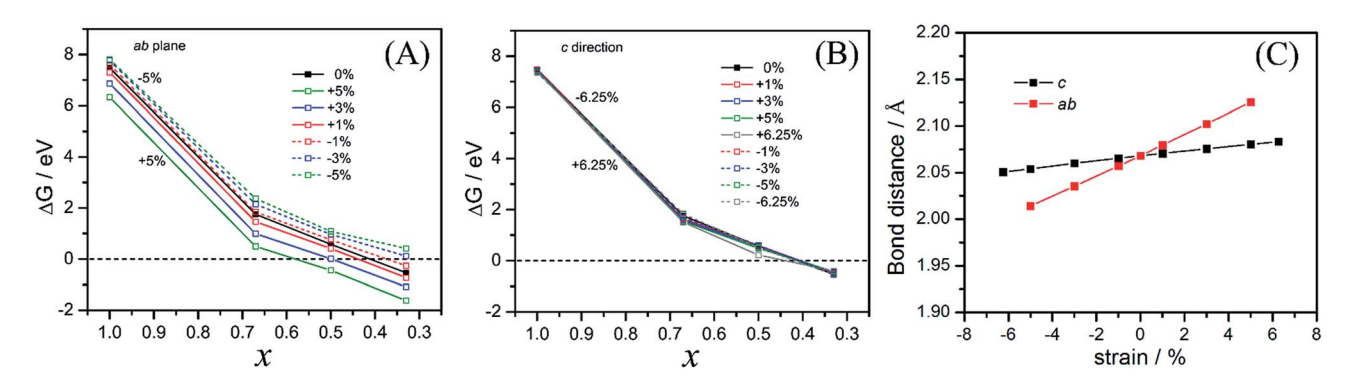


Fig. 6 Effect of the biaxial strain in the ab plane (A) and the uniaxial strain in the c-direction (B) on  $\Delta G$  for the oxygen evolution reaction:  $Na_xFeO_2 \rightarrow Na_xFeO_{2-\delta} + \frac{\theta}{2}O_2$ . Average Fe-O bond length as a function of the strain (C).

hand, the uniaxial strains in the c-direction are found to have negligible effect on the oxygen stability. To explain the contrasting strain-dependent behaviors, we calculate the average length of Fe–O bonds in NaFeO $_2$  as a function of the strains, shown in Fig. 6C. It is found that the average Fe–O bond length depends much more sensitively on the in-plane strains than on the out-of-plane strains. Because the stability of oxygen correlates strongly to the strength of Fe–O bonds, thus the bond lengths, the oxygen stability should also depend more strongly on the in-plane strains than the out-of-plane strains.

Our previous study17 has revealed that Fe ion tends to migrate into the Na layer in Na<sub>x</sub>FeO<sub>2</sub> at a high voltage and when this happens, the Fe ion hinders the transport of Na ions. To examine how strains would affect this behavior, we have calculated the diffusion energy barriers of Na ion under strains in the presence of Fe ion at the Na layer in Na<sub>x</sub>FeO<sub>2</sub> (x = 0.5 and 0.33). As shown in Fig. 2S, $\dagger$  we find that the *c*-direction uniaxial tension reduces the diffusion energy barrier of Na while the inplane biaxial tension increases it. These trends in strain dependence are the same as those in the absence of the Fe ion at the Na layer. However, we note that 3% tension in the c-direction could no longer render Na diffusion barrierless. In other words, the strain effect becomes weaker in the presence of Fe ion at the Na layer. Finally, we observe that the presence of Fe ion at the Na layer decreases the oxygen stability substantially, which, however, could be mitigated by strains, such as an inplane compression or a *c*-direction tension.

#### 4. Conclusions

In summary, we have carried out first-principles calculations to gain atomistic understanding of structural evolution, ion transport and oxygen stability in layered NaFeO2 in the absence and the presence of applied strains. We identify a divacancy assisted diffusion mechanism in the NaO6 slab whose diffusion barrier agrees well to the experimental value. We find that while both the in-plane and out-of-plane strains can modulate the diffusion barrier, the latter has a much greater effect than the former. In particular, we discover that 3% tension in the *c*-direction renders the diffusion barrierless, thus could drastically enhance the rate performance of the electrode. We have examined the structural evolution of NaFeO2 during desodiation and observed an "abnormal" volume expansion as Na ions are removed. Finally, we study the stability of oxygen in the desodiation process and explore how the stability can be tuned by the lattice strains. We reveal that the in-plane compressions can improve oxygen stability while the out-of-plane strains have little effect on it. With a positive Poisson ratio in NaFeO<sub>2</sub>, a tension in the out-ofplane direction yields a compression in the plane, and vice versa. Therefore, if a sufficient in-plane compression is applied to NaFeO<sub>2</sub>, it would stabilize oxygen and at the same time lower the diffusion barrier. A possible strategy of applying desirable strains to the oxide is to fabricate thin-film NaFeO<sub>2</sub> on a hard or soft substrate. Interfacial strains can be transmitted either passively or actively onto NaFeO<sub>2</sub>.

#### Conflicts of interest

There are no conflicts to declare.

#### Acknowledgements

We thank Dr Xuefeng Wang and Dr Yejing Li at University of California San Diego for helpful discussion. This work was supported by the National Science Foundation (DMR-1828019) and the National Key Development Program of China (No. 2015CB251100).

#### References

- 1 F. Sauvage, L. Laffont, J.-M. Tarascon and E. Baudrin, *Inorg. Chem.*, 2007, **46**, 3289.
- 2 D. Kim, E. Lee, M. Slater, W. Lu, S. Rood and C. S. Johnson, *Electrochem. Commun.*, 2012, **18**, 66.
- 3 H. L. Pan, X. Lu, X. Q. Yu, Y. S. Hu, H. Li, X. Q. Yang and L. Q. Chen, Adv. Energy Mater., 2013, 3, 1186.
- 4 S.-M. Oh, S.-T. Myung, J. Hassoun, B. Scrosati and Y.-K. Sun, *Electrochem. Commun.*, 2012, 22, 149.
- 5 S. H. Woo, Y. Park, W. Y. Choi, N. S. Choi, S. Nam, B. Park and K. T. Lee, *J. Electrochem. Soc.*, 2012, **159**, A2016.
- 6 C.-Y. Yu, J.-S. Park, H.-G. Jung, K.-Y. Chung, D. Aurbach, Y.-K. Sun and S.-T. Myung, *Energy Environ. Sci.*, 2015, **8**, 2019.
- 7 C. Delmas, C. Fouassier and P. Hagenmuller, *Physica B+C*, 1980, **99**, 81.
- 8 H. Yoshida, N. Yabuuchi and S. Komaba, *Electrochem. Commun.*, 2013, 34, 60.
- 9 X. Wang, G. Liu, T. Iwao, M. Okubo and A. Yamada, J. Phys. Chem. C, 2014, 118, 2970.
- 10 H. Yoshida, N. Yabuuchi and S. Komaba, Na insertion mechanism in Alpha NaFeO<sub>2</sub> as positive electrode materials for Na-ion batteries, Honolulu PRiME 2012 ECS Abstr., 2012, p. 1850.
- 11 N. Yabuuchi, H. Yoshida and S. Komaba, *Electrochemistry*, 2012, **80**, 716.
- 12 J. Zhao, L. Zhao, N. Dimov, S. Okada and T. Nishida, *J. Electrochem. Soc.*, 2013, **160**, A3077.
- 13 S. Okada, Y. Takahashi, T. Kiyabu, T. Doi, J.-i. Yamaki and T. Nishida, *Layered Transition Metal Oxides as Cathodes for Sodium Secondary Battery*, 210th ECS Abstr., 2006, p. 201.
- 14 Y. Takeda, K. Nakahara, M. Nishijima, N. Imanishi and O. Yamamoto, *Mater. Res. Bull.*, 1994, **29**, 659.
- 15 M. C. Blesa, E. Moran, C. León, J. Santamaria, J. D. Tornero and N. Menéndez, *Solid State Ionics*, 1999, **126**, 81.
- 16 E. Lee, D. E. Brown, E. E. Alp, Y. Ren, J. Lu, J.-J. Woo and C. S. Johnson, *Chem. Mater.*, 2015, 27, 6755.
- 17 Y. J. Li, Y. R. Gao, X. F. Wang, X. Shen, Q. Y. Kong, R. C. Yu, G. Lu, Z. X. Wang and L. Q. Chen, *Nano Energy*, 2018, 47, 519.
- 18 Z. Shadike, Y. N. Zhou, L. L. Chen, Q. Wu, J. L. Yue, N. Zhang, X. Q. Yang, L. Gu, X. S. Liu, S. Q. Shi and Z. W. Fu, *Nat. Commun.*, 2017, 8, 566.
- 19 S. Shi, J. Gao, Y. Liu, Y. Zhao, Q. Wu, W. Ju, C. Ouyang and R. Xiao, *Chin. Phys. B*, 2016, 25, 018212.

- 20 P. Hu, X. Wang, J. Ma, Z. Zhang, J. He, X. Wang, S. Shi, G. Cui and L. Chen, Nano Energy, 2016, 26, 382.
- 21 S. Shi, P. Lu, Z. Liu, Y. Qi, L. G. Hector Jr, H. Li and S. J. Harris, J. Am. Chem. Soc., 2012, 134, 15476.
- 22 S. Shi, H. Zhang, X. Ke, C. Ouyang, M. Lei and L. Chen, Phys. Lett. A, 2009, 373, 4096.
- 23 P. Hohenberg and W. Kohn, Phys. Rev., 1964, 136, B864.
- 24 W. Kohn and L. J. Sham, Phys. Rev., 1965, 140, A1133.
- 25 G. Kresse and J. Furthmiiller, Comput. Mater. Sci., 1996, 6, 15.
- 26 P. E. Blöchl, Phys. Rev. B: Condens. Matter Mater. Phys., 1994, 50, 17953.
- 27 J. P. Perdew, K. Burke and M. Ernzerhof, Phys. Rev. Lett., 1996, 77, 3865.
- 28 S. L. Dudarev, G. A. Botton, S. Y. Savrasov, C. J. Humphreys and A. P. Sutton, Phys. Rev. B: Condens. Matter Mater. Phys., 1998, 57, 1505.
- 29 D. Sheppard, P. Xiao, W. Chemelewski, D. D. Johnson and G. Henkelman, J. Chem. Phys., 2012, 136, 074103.
- 30 D. Sheppard, R. Terrell and G. Henkelman, J. Chem. Phys., 2008, 128, 134106.
- 31 D. Sheppard and G. Henkelman, J. Comput. Chem., 2011, 32,
- 32 F. Zhou, M. Cococcioni, C. A. Marianetti, D. Morgan and G. Ceder, Phys. Rev. B: Condens. Matter Mater. Phys., 2004, 70, 235121.

- 33 W. E. Pickett, S. C. Erwin and E. C. Ethridge, Phys. Rev. B: Condens. Matter Mater. Phys., 1998, 58, 1201.
- 34 C. Delmas, A. Maazaz, C. Fouassier, J.-M. Réau and P. Hagenmuller, Mater. Res. Bull., 1979, 14, 329.
- 35 A. Van der Ven and G. Ceder, J. Power Sources, 2001, 97-98, 529.
- 36 A. Van der Ven and G. Ceder, Electrochem. Solid-State Lett., 2000, 3, 301.
- 37 X. Wang, Y. Gao, X. Shen, Y. Li, Q. Kong, S. Lee, Z. Wang, R. Yu, Y.-S. Hu and L. Chen, Energy Environ. Sci., 2015, 8, 2753.
- 38 J.-S. Kim, C. S. Johnson, J. T. Vaughey, M. M. Thackeray, S. A. Hackney, W. Yoon and C. P. Grey, Chem. Mater., 2004, **16**, 1996.
- 39 D. Y. W. Yu, K. Yanagida, Y. Kato and H. Nakamura, J. Electrochem. Soc., 2009, 156, A417.
- 40 Y. Koyama, I. Tanaka, M. Nagao and R. Kanno, J. Power Sources, 2009, 189, 798.
- 41 J. S. Hummelshoj, J. Blomqvist, S. Datta, T. Vegge, J. Rossmeisl, K. S. Thygesen, A. C. Luntz, K. W. Jacobsen and J. K. Norskov, J. Chem. Phys., 2010, 132, 071101.
- 42 P. Atkins and J. de Paula, Physical Chemistry, Oxford University Press, Oxford, 7th edn, 2002.

This journal is © The Royal Society of Chemistry 2019